Conjugation of Antibodies and siRNA Duplexes to Polymer Nanoparticles via Maleimide–Thiol Chemistry

Elise C. Hoover, Chitran Roy Chowdhury, Olivia M. Ruggiero, and Emily S. Day*

Read Online

ACCESS | Metrics & More | Article Recommendations | Supporting Information

ABSTRACT: Polymeric nanoparticles (NPs) have shown great promise as highly modifiable platforms that can be applied across many different disease states. They are advantageous because they can encapsulate a range of hydrophobic and hydrophilic cargoes while having customizable surface properties. Depending on the desired biointerfacing capabilities, the surface of polymeric NPs can be modified with moieties, such as antibodies, peptides, nucleic acids, and more. The work presented here is intended to provide mechanistic insight into how different parameters influence the loading of antibodies, small interfering ribonucleic acids (siRNAs), or both on the surface of poly(lactic-*co*-glycolic acid) (PLGA) NPs via maleimide−thiol chemistry. Some of the conjugation parameters investigated include the buffer concentration, maleimide to protein ratio, and the addition of an excipient such as Tween-20. Through variation in the concentration of FZD7 antibodies added to the reaction mixture, we established tunable conjugation and found the upper limit of their loading density under the conditions tested. We also confirmed antibody conjugation through two different mechanisms: via a thiol-modified antibody or a thiol-modified poly(ethylene glycol) (PEG) linker. Conjugation of thiolated siRNA duplexes targeting β-catenin was also investigated through variations in both Tween-20 concentration and CaCl₂ buffer concentration. Finally, the coconjugation of both antibodies and siRNA duplexes was explored. Overall, this work outlines a basis for tunable biomolecule loading on polymer NPs using maleimide−thiol chemistry and reveals the incredible versatility of polymer NP platforms.
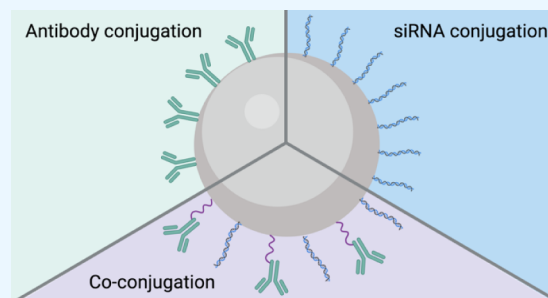
INTRODUCTION

Interest in using nanosized conjugates as novel therapeutics has rapidly grown over the last few decades. Polymeric nanoparticles (NPs) in particular have shown great promise as highly modifiable platforms that can be applied across many different disease states. Polymer NPs loaded with cargos have a wide variety of advantages over nonencapsulated cargos, including longer circulation time, tunable size and charge, and adjustable release kinetics.[1−3] Polymeric NPs are also advantageous because they can encapsulate a range of hydrophobic[4] and hydrophilic[5,6] cargos while having highly customizable surface properties.[2,7] Depending on the desired biointerfacing capabilities, the surface of polymeric NPs can be modified with moieties, such as antibodies, peptides, nucleic acids, and more.[8−11] Possible cargos to be encapsulated within the NPs include small molecule drugs, nucleic acids, fluorescent dyes, and other contrast agents.[12−14] There are many options for polymer materials, including poly(D,L-lactic-*co*-glycolic acid) (PLGA), polyethylenimine (PEI), and polylactic acid (PLA).[15,16] This work focuses on PLGA because it is an FDA-approved, biocompatible, and biodegradable material that has already shown success in clinical trials.[1,15,17]

Due to their versatility, polymer NPs can be used to treat a range of diseases such as arthritis, cancers, neurodegenerative diseases, and a variety of women's health issues including endometriosis, vaginal infections, and pregnancy disorders.[18−22] For cancers in particular, NPs comprised of various materials have shown great promise to provide more efficient and targeted delivery of both therapeutic and diagnostic agents.[21,23] Many types of cancers such as triple-negative breast cancer (TNBC), pancreatic cancer, and cervical cancer require novel targeting approaches because the diseased cells lack expression of common markers that are exploited by the current standards of care in the clinic.[24−26] Improved targeting can be achieved through a variety of methods, including antibodies, cell membrane coatings, peptides, and more.[8,27,28] To use moieties such as antibodies or peptides for receptor-mediated targeting, the molecules need to be conjugated to or otherwise incorporated into the NP surface in a manner that will allow for optimum interactions with cell surfaces and maximal cell binding and uptake. Depending on the desired target, there may be an optimal surface density of the targeting ligand to achieve the greatest level of uptake and/or

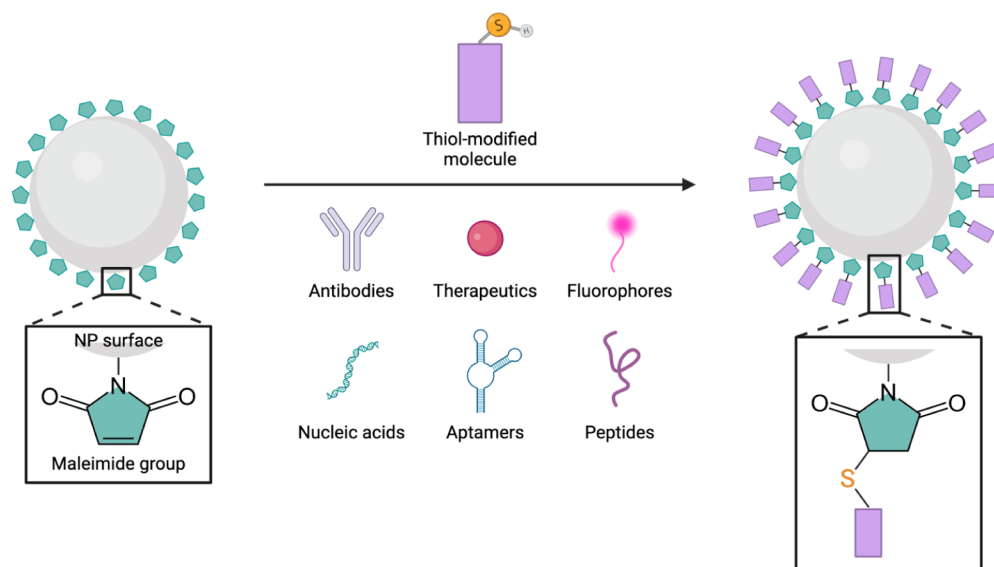**Scheme 1. Polymer NPs Modified with a Maleimide Binding Site Offer a Wide Variety of Options for Potential Cargos to be Conjugated to the Surface via Maleimide-Thiol Chemistry**

therapeutic effect that may not correlate to the maximum number of moieties attached to the NP surface.[9,29] Therefore, the ability to tune the surface loading of these molecules is vital when designing targeted NP platforms.

Other surface modifications often used with polymer NPs include the conjugation of poly(ethylene glycol) (PEG), oligonucleotides, fluorophores, and more. Oligonucleotides in particular are one of the most investigated NP cargos due to the vast promise of gene regulation and the potential for nanoconjugation/encapsulation of nucleic acids to avoid the high levels of enzymatic degradation, phagocytic clearance, and inefficient endosomal escape seen with freely delivered nucleic acids.[6,30] When they are incorporated into an NP structure, either through encapsulation or conjugation, nucleic acids exhibit lower clearance levels and more efficient delivery to disease sites.[31,32]

The conjugation of these various molecules can be complex, with a variety of parameters to consider, therefore necessitating further investigation into the fundamental properties driving these reactions. These conjugations can occur via multiple different chemistries, including carbodiimide, click chemistry, maleimide−thiol, and many more. Maleimide chemistry in particular is favorable due to its highly reactive nature under simple conditions such as room temperature and aqueous buffers, formation of stable bonds, and the wide availability of thiols on DNA strands, peptides, and proteins (Scheme 1).[33−36] While the stability of maleimide−thiol conjugates has been debated due to the potential for maleimide ring opening via hydrolysis, it has also shown greater bonding strength and stability when compared to conjugation via surface adsorption or carbodiimide reactions.[37,38] If desired, the maleimide conjugation can be further stabilized through the use of an *N*-aryl maleimide,[39] incorporating a leaving group into the maleimide scaffold,[40] or adjustments of the binding site to prevent the hydrolysis exchange reaction.[41,42]

The work outlined here is intended to provide mechanistic insight into the optimal conditions for conjugating antibodies, small interfering ribonucleic acids (siRNAs), or both to the surface of PLGA NPs via maleimide−thiol chemistry. Some of the conjugation parameters investigated include buffer

concentration, maleimide to protein ratio, and the addition of an excipient such as Tween-20. $CaCl_2$ is investigated as an alternative buffer to the conventionally used NaCl solutions due to previous studies, indicating enhanced levels of endosomal escape and subsequently more efficient siRNA delivery when siRNA-NP conjugates are prepared in $CaCl_2$ buffer.[43,44] This improved delivery is attributed to greater association of divalent calcium ions with the nucleic acids on the NP surface, which are released from the NPs within endosomes following cellular uptake, thereby inducing a "proton sponge effect" resulting in endosomal destabilization and improved siRNA delivery to the cytosol.[45,46] Based on these prior findings, we wanted to investigate if the use of $CaCl_2$ buffer impacts siRNA or antibody loading efficiency on polymer NPs.

To investigate the various conjugation parameters outlined above, we developed an NP platform designed to target and treat TNBC. As stated earlier, TNBC lacks many of the common clinical markers used to target other forms of cancer. Therefore, new alternative targets need to be used to develop more effective treatments for TNBC. One of these potential targets is the Frizzled7 (FZD7) receptor, which is a key receptor in the Wnt developmental signaling pathway. Cancers that display aberrant Wnt signaling (and overexpressed FZD7) tend to be more aggressive and metastatic with higher levels of recurrence.[47,48] FZD7 is upregulated in TNBC cell lines when compared to non-TNBC cells, making it a promising target to specifically treat TNBC.[49,50] Previous studies have also shown that inhibiting or blocking FZD7 in TNBC cells significantly inhibits cell growth and reduces cell invasion and migration.[49,51,52] The targeting of FZD7 receptors via an antibody-conjugated NP therefore has the potential to both improve specific delivery to TNBC cells as well as inhibit the TNBC cells' oncogenic properties.

In addition to FZD7 receptors, the intracellular protein β-catenin is another appealing target due to its role as one of the key mediators in the Wnt signaling cascade. β-catenin is directly involved in progressing tumorigenesis through its interactions in the nucleus that activate Wnt oncogenes.[53,54] Unfortunately, β-catenin is considered to be "undruggable" due

to its lack of binding sites for small molecules and limited enzymatic activity.[55] While this makes it unsusceptible to many traditional strategies used to target intracellular proteins, it is a promising target for siRNA.[56] Furthermore, because Wnt signaling enhances drug resistance in cancer cells, its selective inhibition has the potential to enhance the effects of a codelivered therapeutic cargo, making this approach highly desirable as a multifaceted treatment.[57,58] In summary, this work investigates the influence of various reaction conditions on the loading of anti-FZD7 antibodies, siRNAs targeting β-catenin (siβcat), or both on PLGA NPs, thereby demonstrating the highly tunable nature of polymer NP bioconjugates for biomedical applications.

■ RESULTS AND DISCUSSION

Characterization of Modified Antibodies. The antibodies used for conjugation were modified through either treatment with 100X tris(2-carboxyethyl) phosphine hydrochloride (TCEP) to reduce disulfide groups in the antibody structure and create free thiols or through the addition of a 5 kDa orthopyridyl disulfide-PEG-succinimidyl valerate (OPSS-PEG-SVA) linker (Figure S1). Ellman's assay was used to validate thiolation following incubation with TCEP of both a generic IgG antibody (IgG-SH) and the anti-FZD7 antibody (FZD7-SH). Quantification of free thiols present on the TCEP-modified antibodies indicated ~4 free thiols per antibody for both the control IgG-SH and the target FZD7-SH, while unmodified antibodies did not indicate any presence of free thiols (Figure 1a). Further characterization of the modified antibodies was performed via sodium dodecyl sulfate polyacrylamide gel electrophoresis (SDS-PAGE) and an enzyme-linked immunosorbent assay (ELISA). SDS-PAGE confirmed that the anti-FZD7 antibody modified with the OPSS-PEG-SVA linker (FZD7-linker) maintained a similar molecular weight to the unmodified antibody (Figure 1b). By comparison, the FZD7-SH appears to be slightly lower in molecular weight than the unmodified antibodies, likely due to some loss of the light chain, as indicated by the faint band present around 27 kDa. To confirm the ability of the modified antibodies to bind to their target cells, an ELISA was used to quantify binding avidity when compared to unmodified anti-FZD7 antibodies (Figure 1c). These results indicated a ~1.5× higher level of binding to MDA-MB-231 human TNBC cells for the FZD7-SH antibodies and comparable binding for the FZD7-linker antibodies with a relative avidity of 0.84.
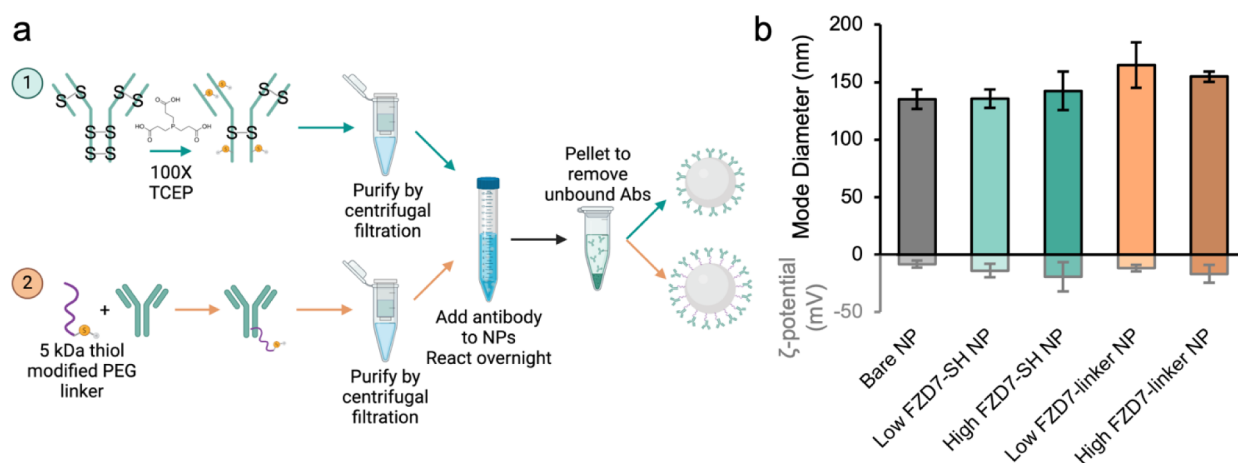
Synthesis of NPs and Conjugation with Antibodies. The NPs used for conjugation were synthesized using a single emulsion oil-in-water protocol (Figure S2a). Briefly, poly-(lactide-co-glycolic acid)−poly(ethylene glycol)−maleimide (PLGA−PEG−Mal) dissolved in dichloromethane (DCM) was added to 0.25% poly(vinyl alcohol) (PVA) in a 1:3 volumetric ratio and probe sonicated on ice. This emulsion was stirred for 4 h allowing for the organic solvent to evaporate. Following solvent evaporation, the NPs were purified via centrifugal filtration. The PVA concentration was chosen based on analysis of varying concentrations, where the 0.25% concentration gave the smallest and most consistent NPs with a diameter of ~135 nm as measured by nanoparticle tracking analysis (NTA) (Figure S2b).

Following optimization of the NP synthesis, FZD7-SH or FZD7-linker antibodies were conjugated to the NP surface using maleimide−thiol chemistry in either a 2 mM ethylenediaminetetraacetic acid (EDTA) buffer or 100 mM CaCl$_2$
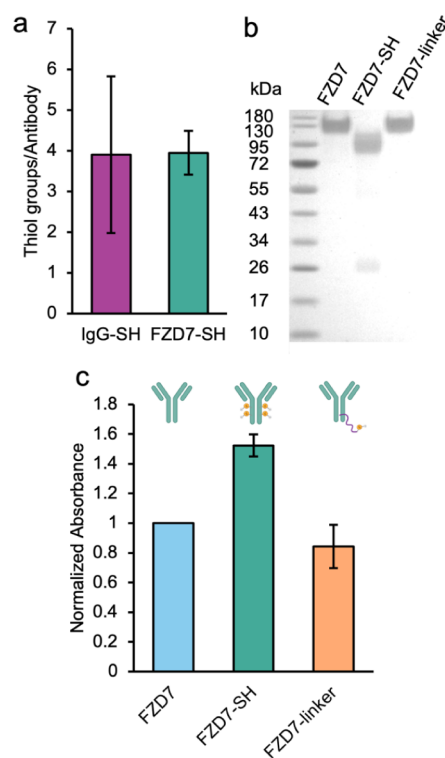
Figure 1. Characterization of modified antibodies. (a) Quantification of free thiols present in antibodies treated with TCEP via Ellman's assay ($n = 3$). Data are the mean ± standard deviation. (b) SDS-PAGE of unmodified anti-FZD7 antibodies, anti-FZD7 antibodies treated with TCEP (i.e., FZD7-SH), and anti-FZD7 antibodies conjugated to an OPSS-PEG-SVA linker (i.e., FZD7-linker). (c) Quantification of antibody binding avidity to MDA-MB-231 cells using an ELISA. Relative binding was normalized to that of the unmodified anti-FZD7 antibodies ($n = 3$). Data are mean ± standard deviation.

buffer (Figure 2a). The buffer containing 2 mM EDTA was selected for evaluation because EDTA is often used for maleimide−thiol reactions due to EDTA's ability to prevent oxidation of free thiols by chelating stray divalent metals.[59−61] The CaCl$_2$ buffer was also chosen for investigation as an alternative salt buffer that is more translatable to interactions with nucleic acids, lending itself to the conjugation of both antibodies and nucleic acids on the NP surface.[43,62] We also tested two different initial loading conditions ("Low" or "High") to determine their influence on the final antibody loading density. The "High" condition was chosen as a maximum saturation of the NP surface based on previous studies using NPs synthesized in the same manner, while the "Low" condition was chosen to use a 3-fold lower level of antibodies as an example of tunability.[63] The loading conditions were controlled by changing the number of antibodies added to the initial conjugation reaction, where the Low and High loading conditions correspond to an initial condition of either 1,000 or 3,000 antibodies per NP, respectively. Based on maleimide content available on the NP surface, the Low loading condition yields a maleimide:antibody ratio of 16:1, while the High loading condition yields a 5:1 ratio. Loading ratios using maleimide−thiol chemistry typically range from 2:1 to 20:1, depending on solution conditions.[37,61]

Figure 2. Synthesis and characterization of antibody-conjugated NPs. (a) Simplified protocol for conjugation of modified FZD7 antibodies to PLGA NPs. (b) Mode diameter and mean zeta potential of NPs conjugated with FZD7 antibodies ($n = 3$). Error bars indicate the standard deviation.

Table 1. Quantification of the Effects of Initial Antibody Loading Concentration, Conjugation Method, and Buffer on the Number of Antibodies Conjugated to NPs

Loading Condition	Conjugation Method	Conjugation Buffer	Antibodies Conjugated/NP	Loading Efficiency (%)	Surface Coverage (%)
Low	TCEP thiolation	2 mM EDTA/PBS	315 ± 199	33 ± 21	27 ± 17
Low	TCEP thiolation	100 mM CaCl$_2$	305 ± 47.3	32 ± 13	26 ± 10
Low	OPSS-PEG-SVA linker	100 mM CaCl$_2$	204 ± 67.0	22 ± 7.1	17 ± 5.7
High	TCEP thiolation	2 mM EDTA/PBS	1,042 ± 198	37 ± 7.0	88 ± 17
High	OPSS-PEG-SVA linker	100 mM CaCl$_2$	399 ± 37.0	15 ± 1.3	36 ± 3.1

The number of antibodies conjugated per NP was calculated using a solution-based ELISA.[63,64] Quantification of FZD7-SH on the NP surface using the 2 mM EDTA buffer demonstrated 315 ± 199 and 1042 ± 198 antibodies/NP for the Low and High loading conditions, indicating tunable antibody loading (Table 1). These levels of conjugation correspond to 27% and 88% surface coverage of the NPs for the Low and High loading conditions, respectively. When an alternate buffer of 100 mM CaCl$_2$ is used, similar levels of conjugation for the Low loading condition were observed with approximately 305 ± 47.3 antibodies/NP, corresponding to 26% surface coverage. The use of the OPSS-PEG-SVA linker showed the least efficient levels of conjugation with only 192 ± 29.7 antibodies/NP under the Low loading condition and 399 ± 37.0 antibodies/ NP under the High loading condition. The antibody loading under the High loading condition using the TCEP thiolation was significantly different from all other groups after analysis using an ANOVA with posthoc Tukey ($p < 0.001$). The most efficient conjugation was observed with the TCEP-modified antibodies and the 2 mM EDTA buffer. One possibility for the lower efficiency of the FZD7-linker conjugation could be the presence of only one free thiol group on the PEG linker, while the FZD7-SH antibodies have approximately 4 free thiols per antibody. This higher presence of free thiols could give the FZD7-SH antibodies an advantage by creating more potential interaction sites to react with the maleimide groups on the NP surface. Another possibility for the lower efficiency could be that once any initial FZD7-linker binds to the surface, the physical presence of the linker could create steric hindrance to limit further interactions with the maleimide groups. Regarding stability of the conjugates, we observed little to no antibody loss from the Low FZD7-SH NPs over time, with loading of 348 ± 146 antibodies per NP measured after 1 week of
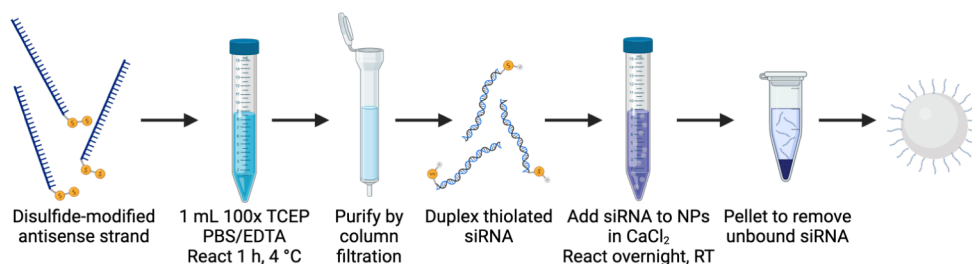
incubation in water at 4 °C ($n = 3$). This analysis was not performed for the other conditions, but we anticipate similar stability based on the comparable chemistries used to tether the antibodies to the NPs.

NTA quantification of NP mode diameter pre- and post-antibody conjugation indicates an ∼0 to 10 nm shift following conjugation with low or high amounts of FZD7-SH and a shift of ∼20 to 30 nm following conjugation with FZD7-linker (Figure 2b). The bare NPs had a hydrodynamic diameter of 135 ± 8.6 nm, while the Low FZD7-SH NPs were 135 ± 8.0 nm and the High FZD7-SH NPs were approximately 142 ± 17 nm. The FZD7-linker NPs had diameters of 165 ± 20 nm and 155 ± 4.4 nm for the Low and High conditions, respectively. The minimal shift in diameter for the FZD7-SH conjugation method can likely be attributed to a nondirectional conjugation of the antibodies to the NP surface. Since free thiols are scattered across the antibody backbone, the conjugation may have occurred at any of those sites. Despite the approximate length of an IgG-based antibody being ∼10−14 nm,[65] we do not observe this same shift in diameter due to the nondirectional nature of this conjugation method. It is also possible that the nature of hydrodynamic diameter measurements, including both the NP and ions associated with the NP may mask some of the size increase due to the antibody attachment.

The zeta potential shifts from −8.3 mV for bare NPs to −14 mV for the FZD7-SH Low loading condition and to −19 mV for the FZD7-SH High loading condition, while the FZD7-linker Low loading condition had a zeta potential of −11 mV and the FZD7-linker Low loading condition had a zeta potential of −17 mV. The slightly more negative zeta potentials of the antibody-conjugated NPs can likely be

Scheme 2. Simplified Protocol for siRNA Conjugation to Maleimide-Modified Polymer NPs

Disulfide-modified antisense strand → 1 mL 100x TCEP PBS/EDTA React 1 h, 4 °C → Purify by column filtration → Duplex thiolated siRNA → Add siRNA to NPs in CaCl₂ React overnight, RT → Pellet to remove unbound siRNA

Table 2. Quantification of the Effects of Tween-20 Concentration and CaCl₂ Buffer Concentration on the Amount of siRNA Conjugated to NPs

Tween-20 Concentration (%)	CaCl₂ Concentration (mM)	RNA Loading (μg RNA/mg PLGA)	Loading Efficiency (%)	Zeta Potential (mV)	Mode Diameter (nm)
0	50	1.6 ± 0.5	11.2 ± 3.3	-25.1 ± 3.5	162.6 ± 21
0	100	1.6 ± 0.5	11.1 ± 3.4	-23.3 ± 6.1	172.9 ± 19
0	225	1.5 ± 0.6	9.2 ± 4.9	-11.3 ± 5.4	180.9 ± 11
0.05	100	1.8 ± 0.1	12.1 ± 0.9	-13.5 ± 12	153.1 ± 14.4
0.1	100	2.7 ± 0.7	18.8 ± 5.1	-21.4 ± 8.5	163.4 ± 12.8
0.5	100	1.9 ± 0.9	13.1 ± 6.2	-15.5 ± 8.8	167.2 ± 25.4
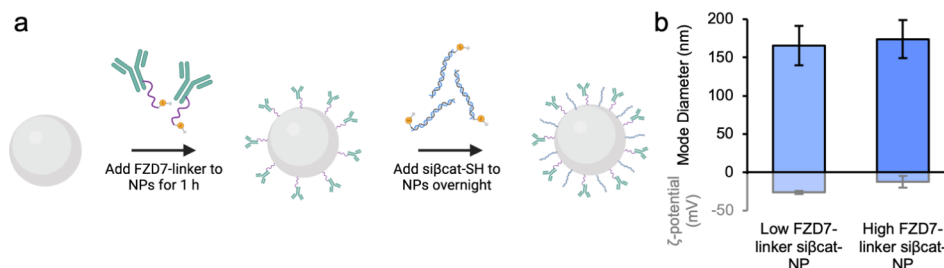
Figure 3. Synthesis and characterization of NPs modified with both antibodies and siRNAs. (a) Simplified protocol for coconjugation of FZD7-linker antibodies and siβcat siRNAs. (b) Mode diameter and zeta potential of NPs conjugated with both FZD7-linker antibodies and siβcat siRNAs ($n = 3$). Error bars indicate standard deviation.

attributed to any charged thiolates remaining on the antibodies.[66]

Conjugation of siRNA to the NP Surface. The core polymer NPs used for siRNA conjugation were synthesized in the same manner as that described above. The conjugation was performed using a reduced disulfide modification on the antisense strand before being duplexed with the corresponding sense strand and being added to the NPs in a CaCl₂ solution (Scheme 2).

Different concentrations of CaCl₂ were investigated including 50, 100, and 225 mM as well as different concentrations of Tween-20 including 0%, 0.05%, 0.1%, and 0.5% (Table 2). Varying the CaCl₂ concentration did not have a significant effect on the siβcat conjugation. However, at the highest concentration of 225 mM, a slight decrease in loading efficiency was noted where it dropped from ~11% for the 50 and 100 mM concentrations to ~9% for the 225 mM concentration. The NPs synthesized in the 225 mM concentration also had the largest diameter of the three concentrations. Bare NPs that underwent the same incubation conditions had a diameter of 159.2 ± 5.0 nm, indicating an average diameter shift of ~10 nm following siRNA conjugation. No statistical significance comparing RNA loading was found between groups using an ANOVA.

The addition of Tween-20 moderately improved the siβcat conjugation with the highest loading efficiency seen at the

0.1% concentration at almost 19%, corresponding to 2.7 ± 0.7 μg of RNA/mg of PLGA. Concentrations higher than 0.1% started to decrease the siβcat loading efficiency. The zeta potentials of the NPs incubated with Tween were slightly more neutral, which can likely be attributed to Tween's ability to suppress surface charge.[67−69] Because the zeta potential of the 0.5% condition is similar to the 0.05% condition, we believe that the Tween has maximized its interactions with the NP surface at the lower concentration; hence, additional Tween does not continue to change the zeta potential. We attribute the more negative zeta potential of the 0.1% Tween condition to the presence of more siRNA on the NP surface.

Combined Conjugation of Antibodies and siRNA to the NP Surface. To investigate the potential to load multiple types of molecules on an NP surface, the PLGA NPs were incubated with both the FZD7-linker antibodies and the siβcat siRNAs in 100 mM CaCl₂ buffer containing 0.1% Tween-20. Briefly, the NPs were first incubated with the FZD7-linker antibodies for 1 h in either the Low or High loading conditions before adding 1 nmol of siβcat per milligram of NPs (Figure 3a). The linker-modified FZD7 was chosen for this conjugation to provide more available space near the NP surface to allow for coloading of siRNA.

When adding the FZD7-linker to the NPs in the Low condition, similar siβcat loading was seen when compared to the NPs that lack FZD7 with 2.7 μg of RNA/mg of PLGA

(Table 3). We also found similar antibody loading when compared to the FZD7-linker NPs that lacked siβcat with a

Table 3. Quantification of the Combined Antibody and siRNA Loading on NPs

Antibody Loading Condition	RNA Loading (μg RNA/mg PLGA)	RNA Loading Efficiency (%)	Antibodies Conjugated/NP	Antibody Loading Efficiency (%)
Low	2.7 ± 0.4	19 ± 2.7	229 ± 33.7	24 ± 3.6
High	2.0 ± 0.2	14 ± 1.5	358 ± 77.3	13 ± 2.7

value of approximately 229 antibodies/NP. When the antibodies were added in the High loading condition, the RNA loading decreased to 2.0 μg RNA/mg PLGA while the antibodies conjugated increased to 358 antibodies/NP. Both the RNA and antibody loading for the High condition were significantly different from the Low loading condition using a t test ($p < 0.05$). An increase in diameter when compared to the Bare NPs was also found with values of 166 ± 25.8 and 174 ± 24.9 nm for the Low and High loading conditions, respectively (Figure 3b). The zeta potential is slightly more neutral under the High loading condition, yielding a value of −12.3 ± 7.8 mV when compared to −26.2 ± 1.8 mV for the Low loading condition. This shift is likely due to the slightly lower level of RNA loading under the High loading condition, so the RNA charge has less of an effect on the overall zeta potential and therefore leads to a more positive value.

■ CONCLUSIONS

The findings in this work demonstrate the importance of investigating protocol parameters to achieve optimal bioconjugation to NPs. Through variation in initial loading content of FZD7 antibodies, we established the tunable nature of polymer NPs and found the upper limit of their conjugation under the conditions tested. We also confirmed antibody conjugation through two different mechanisms: via a thiol-modified antibody or a thiol-modified PEG-linker. Contrary to our initial expectation, the thiol modification directly on the antibodies after incubation with TCEP proved to be more efficient for conjugation to the NP surface than attachment via PEG linkers. Conjugation of siβcat siRNA duplexes was also investigated through variations in both Tween-20 concentration and CaCl$_2$ buffer concentration. Optimal siRNA loading was found using 0.1% Tween-20 and 100 mM CaCl$_2$ concentration. Finally, the coconjugation of the two different molecules was explored. After an initial incubation with the FZD7-linker antibodies, siβcat was also added to create a dual-loaded NP. With increased loading of the FZD7-linker antibodies, decreased conjugation of siβcat was seen. Overall, the work presented here outlines a basis for how conjugation parameters impact attachment of two different biomolecules to polymer NPs via maleimide−thiol chemistry and reveals the high versatility of polymer NP bioconjugates.

■ MATERIALS AND METHODS

Thiolation of Antibodies. Either normal rabbit IgG (2729S, Cell Signaling Technology) or rabbit anti-human FZD7 antibodies (LS-C383580, LSBio) were used. To modify the antibodies, they were first incubated with a 100× molar excess of TCEP (Sigma-Aldrich) in phosphate buffered saline (PBS) containing 2 mM EDTA (ThermoFisher) for 1 h at 4 °C on a rocker. Following incubation with TCEP, the antibodies were washed three times in 10 kDa Corning Spin-X UF (Sigma-Aldrich) concentrators for 10 min at 12,000 rcf, 4 °C with PBS to remove excess TCEP.

Preparation of FZD7-Linker Antibodies. To attach a linker to the anti-FZD7 antibodies, a 5 kDa OPSS-PEG-SVA linker was first reconstituted in 100 mM sodium bicarbonate before being incubated with 100× molar excess TCEP for 1 h at 4 °C on a rocker to break the disulfide bond and create a free thiol (Figure S1). The thiolated linker was then incubated with the anti-FZD7 antibodies in a 2:1 PEG:antibody molar ratio overnight on a rocker at 4 °C. Following overnight incubation, the antibodies were washed thrice in 10 kDa Corning Spin-X UF concentrators for 10 min at 12,000 rcf, 4 °C with PBS to remove unbound linker.

Characterization of Thiolated Antibodies and Linker Antibodies. To quantify free thiols in the IgG-SH and FZD7-SH antibodies, Ellman's Assay was used (Sigma-Aldrich). Per the manufacturer's instructions, antibody samples were prepared in 50 μL at 0.5 mM before adding 500 μL of a reaction buffer consisting of 1 mM EDTA in PBS. A standard curve was prepared using L-cysteine hydrochloride monohydrate (Sigma-Aldrich) ranging from 0 to 1.5 mM in 50 μL volumes before adding 500 μL of the reaction buffer. The Ellman's reagent solution (Sigma-Aldrich), also known as 5,5′-dithio-bis(2-nitrobenzoic acid) (DTNB), was prepared in PBS at a 4 mg/mL concentration. The antibody samples and standards were then incubated with 10 μL of Ellman's reagent solution for 15 min at room temperature. The samples were plated in triplicate 100 μL volumes in a 96-well plate, and the absorbance was read at 412 nm using a Synergy H1 plate reader (BioTek). Thiol levels in the antibodies were calculated based on the standard curve.

To assess antibody structure post modification, sodium dodecyl sulfate (SDS)-polyacrylamide gel electrophoresis (PAGE) was performed on unmodified, thiolated (i.e., FZD7-SH), and PEGylated antibodies (i.e., FZD7-linker). Samples were diluted to 10 μg of antibody in 1× PBS and 2× Laemmli Concentrate (Sigma-Aldrich) per well in 4−12% Bolt Bis-Tris Plus gels (ThermoFisher) with one well containing a prestained 11−250 kDa protein ladder (Cell Signaling Technology). Running buffer was prepared by making a 1× stock of 3-(N-morpholino) propanesulfonic acid (MOPS; ThermoFisher). The gel was loaded into a minigel tank (ThermoFisher) filled with the 1× MOPS buffer and run at 120 V for 75 min. Any empty wells were filled with a 1× Laemmli solution of equivalent volume. The gel was then removed, rinsed with reverse osmosis purified (RO) water, and stained with SimplyBlue SafeStain (ThermoFisher) for 1 h at room temperature on a rocker. After the stain incubation, the solution was discarded and the gel was rinsed in RO water for 30 min while rocking at room temperature. The RO water was then discarded again, and new RO water was added to wash the gel overnight while rocking at 4 °C. After the gel was rinsed overnight, it was placed on transparency paper and imaged for qualitative analysis.

Binding avidity of the FZD7 antibodies to MDA-MB-231 cells was analyzed using an Enzyme Linked Immunosorbent Assay (ELISA). MDA-MB-231 cells (cultured as described in "Cell culture") were plated at 15,000 cells per well in a 96-well plate. Following overnight incubation, cells were fixed with 4% formaldehyde and washed three times with 1× PBS. Cells were then treated with 3% hydrogen peroxide for 10 min before blocking with PBS containing 3% bovine serum albumin

(PBSA) for 2 h. Samples were next incubated with 50 nM either unmodified anti-FZD7 antibodies or modified FZD7-SH or FZD7-linker antibodies and incubated at room temperature for 1 h on a rocker. Samples were then washed 3× for 10 min with 1% PBSA (i.e., 1% bovine serum albumin in PBS) containing 0.01% Tween-20 (PBST). Following wash steps, samples were treated with 2.5 μg/mL HRP-conjugated antirabbit secondary antibodies (FisherSci) for 1 h. Samples were washed three times with PBST before developing the reaction with 3,3′,5,5′-tetramethylbenzidine (TMB, Bio-Rad). 2 M sulfuric acid was added to stop the reaction. Absorbance was measured at 450 nm by using a Synergy H1 plate reader. Samples were normalized to the signal of unmodified anti-FZD7 antibodies. Samples that were not treated with primary antibodies displayed negligible levels of the signal. These experiments were performed in at least triplicate.

Cell Culture. MDA-MB-231 human TNBC cells (American Type Culture Collection, ATCC) were cultured in Dulbecco's Modified Eagle Medium (DMEM; Fisher Scientific) supplemented with 10% fetal bovine serum (FBS; Gemini Bio Products) and 1% penicillin-streptomycin (pen-strep; VWR). Cells were cultured in T75 cell culture flasks at 37 °C in a 5% CO_2 environment. Cells were passaged or plated when they reached 80−90% confluency and were detached from the flask using 3 mL of 0.25% Trypsin-EDTA (ThermoFisher). Cells were counted using a hemocytometer.

Synthesis of NPs. PLGA−PEG−Mal NPs were synthesized using a single emulsion oil-in-water method. PLGA−PEG−Mal (20 kDa 50:50 PLGA, 5 kDa PEG, Nanosoft Polymers) was dissolved in dichloromethane (DCM) at a concentration of 2 mg/mL. 1 mL portion of the PLGA−PEG−Mal/DCM solution was added to 3 mL of either 0.1%, 0.25%, or 0.5% PVA dissolved in PBS. This oil-in-water solution was then probe sonicated on ice with a Fisherbrand model 120 Sonic Dismembrator (Fisher Scientific) at 80% amplitude for 60 s (10 s on, 5 s off). The DCM solvent was allowed to evaporate for 4 h at room temperature with continuous stirring at 800 rpm. Following solvent evaporation, the resulting NPs were purified to remove excess solvent using Millipore 10 kDa molecular weight cutoff (MWCO) filters (4200 g, 30 min, 4 °C) once then transferred to 2 mL Eppendorf tubes, resuspended in 2 mL of Milli-Q water, and centrifuged for 15 min at 20,000 rcf at 4 °C to pellet the NPs. The supernatant was removed, and the NP pellet was resuspended in 2 mL of fresh Milli-Q water and washed once more before being resuspended in 200 μL Milli-Q water.

Maleimide Group Quantification. Quantification of available maleimide binding sites on the NP surface was performed by using a Colorimetric Maleimide Assay Kit (Sigma-Aldrich). Briefly, an excess of free thiols in the form of 1× MEA (2-aminoethanethiol hydrochloride) was added either to a control buffer solution (provided in the kit) or to 0.05 mg of bare NPs suspended in the buffer solution. The remaining free thiols that did not react with the maleimide were quantified after adding 1× 4,4′-dithiodipyridine to the solution by reading the absorbance at 324 nm on a Synergy H1 plate reader. The amount of maleimide was calculated as the difference between the initial amount of free thiol and the amount of unreacted thiol following incubation with the maleimide-NPs.

Conjugation of Thiolated Antibodies to NPs. To conjugate antibodies to the NP surface, thiol-modified antibodies were incubated with the NPs in either PBS containing 2 mM EDTA or Milli-Q water containing 100 mM calcium chloride ($CaCl_2$, Sigma-Aldrich) overnight on a rocker at 4 °C. The NP concentration in the solution was 1 mg/mL. Next, 10 μg of either IgG-SH, FZD7-SH, or FZD7-linker was added per mg of NP for the Low loading condition, and 30 μg of either IgG-SH, FZD7-SH, or FZD7-linker was added per mg of NP for the High loading condition. After overnight incubation while rocking at 4 °C, the NP solution was centrifuged for 15 min at 20,000 rcf at 4 °C to pellet the NPs and remove any unconjugated antibody left in the supernatant. The NP pellet was resuspended in Milli-Q water and washed twice more.

Nanoparticle Characterization. A LiteSizer 500 (Anton-Paar) dynamic light scattering (DLS) instrument was used to measure the polydispersity index and zeta potential of samples diluted in Milli-Q water. A NanoSight NS300 (Malvern Panalytical) nanoparticle tracking analysis system (NTA) was used to measure the diameter and the NP sample concentration (particles/mL) when diluted in Milli-Q water. NP samples were prepared for NTA measurement by diluting a fraction of each sample into 1 mL of Milli-Q water to give a particle count between 20 and 100 particles per frame when introduced to the system. The camera level and focus were adjusted for each sample such that 20% of the visible NPs showed signal saturation, and there were few "halos" around the NPs. A syringe pump injected the samples at an infusion rate of 50−60 A.U. Three 30 s videos recorded by the NTA were used to calculate NP concentrations and diameters. The detection threshold was also adjusted so that the blue crosshair count was less than five for each frame.

Antibody Quantification. Antibody loading on the NP surface was quantified using a solution-based ELISA.[64] Antibody-conjugated NPs were incubated with 10 μg/mL Alexa Fluor 488-conjugated goat anti-rabbit IgG (Thermo-Fisher) in PBS containing 3% bovine serum albumin (3% PBSA) for 1 h at room temperature. Samples were pelleted by centrifugation three times (20,000 rcf, 15 min) to remove unbound secondary antibodies in the supernatant and then resuspended in 3% PBSA. Absorbance at 488 nm was measured on a Synergy H1 plate reader and compared to a standard curve of known Alexa Fluor 488-conjugated goat anti-rabbit IgG concentration to calculate the number of antibodies per NP. The number of NPs per sample was obtained using NTA.

Surface coverage of the NPs was calculated by dividing the total antibody area by the NP surface area. The cross-sectional area of the antibody was assumed to be ∼60 nm^2 due to the width of the antibody across the Fab region being ∼15 nm and the width of the Fc region being ∼4 nm. The total number of antibodies loaded on the surface was multiplied by the antibody cross-sectional area to calculate the total antibody surface area, while the bare NP surface area was calculated using $SA = 4\pi r^2$.

Preparation of siRNA. β-catenin oligonucleotides were purchased as separate sense and antisense strands from Integrated DNA Technologies (IDT). The sense strands had a 3′ thiol modification to allow for conjugation via maleimide−thiol chemistry (Figure S3). Upon resuspension of the separate oligonucleotides in duplex buffer (IDT), the sense strand was treated with 100× molar excess TCEP for 1 h at 4 °C on a rocker to break the disulfide bond and create a free thiol group. After the disulfide reduction, an equimolar amount of the complementary antisense strand was added, and the solution

was heated at 95 °C for 5 min in a thermomixer and then slowly cooled to 37 °C over 1 h to facilitate duplexing. The final siRNA concentration was measured using a Thermo Scientific NanoDrop One Microvolume UV–Vis Spectrophotometer.

Conjugation of siRNA to NPs. To conjugate siRNA to the NP surface, thiol-modified β-catenin siRNA (siβcat) was incubated with the NPs (at a concentration of 1 mg/mL) in either 50, 100, or 225 mM calcium chloride (CaCl$_2$, Sigma-Aldrich) containing either 0%, 0.05%, 0.1%, or 0.5% Tween-20 (Sigma-Aldrich) with overnight stirring at 800 rpm and kept at room temperature. siβcat was added to the NP solution in a ratio of 1 nmol per mg NP. Following overnight incubation, the NP solution was transferred to 1.5 mL Eppendorf tubes and centrifuged for 15 min at 20,000 rcf at 4 °C to pellet the NPs and remove any unconjugated siRNA left in the supernatant. The NP pellet was resuspended in Milli-Q water and washed twice more.

siRNA Quantification. siβcat loading on the NPs was measured using Quant-iT PicoGreen dsDNA Reagent (ThermoFisher). siβcat-NPs were diluted to 1 mg NPs/mL in Milli-Q water containing 10 mM Tris-HCl (ThermoFisher) and 1 mM EDTA. This solution was plated in triplicate for each sample, and the PicoGreen dye (diluted per manufacturer instructions) was added in equal volume. The plate was analyzed with 480 nm excitation/520 nm emission using a Synergy H1 Microplate Reader. The fluorescence was compared to a standard curve of known siβcat concentration.

Combined Conjugation of Antibodies and siRNA to NPs. To conjugate both antibodies and siβcat to the NP surface, NPs were first suspended in 0.1% Tween-20, 100 mM CaCl$_2$ buffer to a concentration of 1 mg/mL. FZD7-linker antibodies were then added to the solution and allowed to stir at 800 rpm for 1 h at room temperature before adding 1 nmol siβcat per mg NP. The solution was left to stir overnight at room temperature. Following overnight incubation, the NP solution was transferred to 1.5 mL Eppendorf tubes and centrifuged for 15 min at 20,000 rcf, 4 °C to pellet the NPs and remove any unconjugated FZD7-linker or siβcat left in the supernatant. The NP pellet was resuspended in Milli-Q water and washed twice more. Antibody and siRNA loading densities were quantified by ELISA and PicoGreen assay, respectively, as described above for the NPs coated with only a single agent.

ASSOCIATED CONTENT

Ⓢ Supporting Information

The Supporting Information is available free of charge at https://pubs.acs.org/doi/10.1021/acsomega.4c07025.

> Figure S1: scheme of OPSS-PEG-SVA modification of antibodies; Figure S2: synthesis of PLGA–PEG–Mal NPs; Figure S3: sequences for siβcat siRNA (PDF)

AUTHOR INFORMATION

Corresponding Author

    Emily S. Day − *Department of Biomedical Engineering, University of Delaware, Newark, DE 19713, United States; Department of Materials Science and Engineering, University of Delaware, Newark, DE 19713, United States; Helen F. Graham Cancer Center and Research Institute, Newark, DE 19713, United States;* ⓞ orcid.org/0000-0002-8707-826X; Email: emilyday@udel.edu

Authors

    Elise C. Hoover − *Department of Biomedical Engineering, University of Delaware, Newark, DE 19713, United States;* ⓞ orcid.org/0000-0003-4723-7446

    Chitran Roy Chowdhury − *Department of Biomedical Engineering, University of Delaware, Newark, DE 19713, United States*

    Olivia M. Ruggiero − *Department of Biomedical Engineering, University of Delaware, Newark, DE 19713, United States;* Present Address: United States Patent & Trademark Office (USPTO), 600 Dulany St, Alexandria VA 22314

Complete contact information is available at:
https://pubs.acs.org/10.1021/acsomega.4c07025

Author Contributions

E.C.H. contributed to data collection, methodology, analysis, visualization, and writing−original draft and editing. C.R.C. contributed to data collection and analysis. O.M.R. contributed to data collection and analysis. E.S.D. contributed to supervision, visualization, writing−review and editing, project administration, and funding acquisition. All authors have given approval to the final version of the manuscript.

Notes

The authors declare no competing financial interest.

■ ACKNOWLEDGMENTS

■ REFERENCES

(1) Anselmo, A. C.; Mitragotri, S. Nanoparticles in the Clinic. *Bioeng. Transl. Med.* **2016**, *1* (1), 10−29.

(2) Mitchell, M. J.; Billingsley, M. M.; Haley, R. M.; Wechsler, M. E.; Peppas, N. A.; Langer, R. Engineering Precision Nanoparticles for Drug Delivery. *Nat. Rev. Drug Discovery* **2021**, *20* (2), 101−124.

(3) Blanco, E.; Shen, H.; Ferrari, M. Principles of Nanoparticle Design for Overcoming Biological Barriers to Drug Delivery. *Nat. Biotechnol.* **2015**, *33* (9), 941−951.

(4) Wilkosz, N.; Łazarski, G.; Kovacik, L.; Gargas, P.; Nowakowska, M.; Jamróz, D.; Kepczynski, M. Molecular Insight into Drug-Loading Capacity of PEG−PLGA Nanoparticles for Itraconazole. *J. Phys. Chem. B* **2018**, *122* (28), 7080−7090.

(5) Jackson, M. A.; Bedingfield, S. K.; Yu, F.; Stokan, M. E.; Miles, R. E.; Curvino, E. J.; Hoogenboezem, E. N.; Bonami, R. H.; Patel, S. S.; Kendall, P. L.; Giorgio, T. D.; Duvall, C. L. Dual Carrier-Cargo Hydrobization and Charge Ratio Optimization Improve the Systemic Circulation and Safety of Zwitterionic Nano-Polyplexes. *Biomaterials* **2019**, *192*, 245−259.

(6) Huang, J.; Xiao, K. Nanoparticles-Based Strategies to Improve the Delivery of Therapeutic Small Interfering RNA in Precision Oncology. *Pharmaceutics* **2022**, *14* (8), 1586.

(7) Correa, S.; Boehnke, N.; Barberio, A. E.; Deiss-Yehiely, E.; Shi, A.; Oberlton, B.; Smith, S. G.; Zervantonakis, I.; Dreaden, E. C.; Hammond, P. T. Tuning Nanoparticle Interactions with Ovarian Cancer through Layer-by-Layer Modification of Surface Chemistry. *ACS Nano* **2020**, *14* (2), 2224−2237.

(8) Dang, M. N.; Hoover, E. C.; Scully, M. A.; Sterin, E. H.; Day, E. S. Antibody Nanocarriers for Cancer Management. *Curr. Opin. Biomed. Eng.* **2021**, *19*, 100295.

(9) Liu, D.; Guo, P.; McCarthy, C.; Wang, B.; Tao, Y.; Auguste, D. Peptide Density Targets and Impedes Triple Negative Breast Cancer Metastasis. *Nat. Commun.* **2018**, *9* (1), 2612.

(10) Zhu, S.; Xing, H.; Gordiichuk, P.; Park, J.; Mirkin, C. A. PLGA Spherical Nucleic Acids. *Adv. Mater.* **2018**, *30* (22), 1707113.

(11) Chaudhari, D.; Kuche, K.; Yadav, V.; Ghadi, R.; Date, T.; Bhargavi, N.; Jain, S. Exploring Paclitaxel-Loaded Adenosine-Conjugated PEGylated PLGA Nanoparticles for Targeting Triple-Negative Breast Cancer. *Drug Delivery Transl. Res.* **2023**, *13*, 1074.

(12) Jin, M.; Hou, Y.; Quan, X.; Chen, L.; Gao, Z.; Huang, W. Smart Polymeric Nanoparticles with pH-Responsive and PEG-Detachable Properties (II): Co-Delivery of Paclitaxel and VEGF siRNA for Synergistic Breast Cancer Therapy in Mice. *Int. J. Nanomed.* **2021**, *2021*, 5479−5494.

(13) Scully, M. A.; Wilhelm, R.; Wilkins, D. E.; Day, E. S. Membrane-Cloaked Nanoparticles for RNA Interference of β-Catenin in Triple-Negative Breast Cancer. *ACS Biomater. Sci. Eng.* **2024**, *10* (3), 1355−1363.

(14) Ong, S. Y.; Zhang, C.; Dong, X.; Yao, S. Q. Recent Advances in Polymeric Nanoparticles for Enhanced Fluorescence and Photoacoustic Imaging. *Angew. Chem., Int. Ed.* **2021**, *60* (33), 17797−17809.

(15) Alsaab, H. O.; Alharbi, F. D.; Alhibs, A. S.; Alanazi, N. B.; Alshehri, B. Y.; Saleh, M. A.; Alshehri, F. S.; Algarni, M. A.; Almugaiteeb, T.; Uddin, M. N.; Alzhrani, R. M. PLGA-Based Nanomedicine: History of Advancement and Development in Clinical Applications of Multiple Diseases. *Pharmaceutics* **2022**, *14* (12), 2728.

(16) Bolhassani, A.; Javanzad, S.; Saleh, T.; Hashemi, M.; Aghasadeghi, M. R.; Sadat, S. M. Polymeric Nanoparticles. *Hum. Vaccines Immunother.* **2014**, *10* (2), 321−332.

(17) Liu, Y.; Cheng, W.; Xin, H.; Liu, R.; Wang, Q.; Cai, W.; Peng, X.; Yang, F.; Xin, H. Nanoparticles Advanced from Preclinical Studies to Clinical Trials for Lung Cancer Therapy. *Cancer Nanotechnol.* **2023**, *14* (1), 28.

(18) Johnson, W. T.; McBride, D.; Kerr, M.; Nguyen, A.; Zoccheddu, M.; Bollmann, M.; Wei, X.; Jones, R. M.; Wang, W.; Svensson, M. N. D.; Bottini, N.; Shah, N. J. Immunomodulatory Nanoparticles for Modulating Arthritis Flares. *ACS Nano* **2024**, *18* (3), 1892−1906.

(19) Cunha, A.; Gaubert, A.; Latxague, L.; Dehay, B. PLGA-Based Nanoparticles for Neuroprotective Drug Delivery in Neurodegenerative Diseases. *Pharmaceutics* **2021**, *13* (7), 1042.

(20) Yu, Z.; Shen, X.; Yu, H.; Tu, H.; Chittasupho, C.; Zhao, Y. Smart Polymeric Nanoparticles in Cancer Immunotherapy. *Pharmaceutics* **2023**, *15* (3), 775.

(21) Bertrand, N.; Wu, J.; Xu, X.; Kamaly, N.; Farokhzad, O. C. Cancer Nanotechnology: The Impact of Passive and Active Targeting in the Era of Modern Cancer Biology. *Adv. Drug Delivery Rev.* **2014**, *66*, 2−25.

(22) Swingle, K. L.; Ricciardi, A. S.; Peranteau, W. H.; Mitchell, M. J. Delivery Technologies for Women's Health Applications. *Nat. Rev. Bioeng.* **2023**, *1* (6), 408−425.

(23) Dancy, J. G.; Wadajkar, A. S.; Connolly, N. P.; Galisteo, R.; Ames, H. M.; Peng, S.; Tran, N. L.; Goloubeva, O. G.; Woodworth, G. F.; Winkles, J. A.; Kim, A. J. Decreased Nonspecific Adhesivity, Receptor-Targeted Therapeutic Nanoparticles for Primary and Metastatic Breast Cancer. *Sci. Adv.* **2020**, *6* (3), No. eaax3931.

(24) Bauer, K. R.; Brown, M.; Cress, R. D.; Parise, C. A.; Caggiano, V. Descriptive Analysis of Estrogen Receptor (ER)-Negative, Progesterone Receptor (PR)-Negative, and HER2-Negative Invasive Breast Cancer, the so-Called Triple-Negative Phenotype. *Cancer* **2007**, *109* (9), 1721−1728.

(25) Leroux, C.; Konstantinidou, G. Targeted Therapies for Pancreatic Cancer: Overview of Current Treatments and New Opportunities for Personalized Oncology. *Cancers* **2021**, *13* (4), 799.

(26) Burmeister, C. A.; Khan, S. F.; Schäfer, G.; Mbatani, N.; Adams, T.; Moodley, J.; Prince, S. Cervical Cancer Therapies: Current Challenges and Future Perspectives. *Tumour Virus Res.* **2022**, *13*, 200238.

(27) Farokhzad, O. C.; Cheng, J.; Teply, B. A.; Sherifi, I.; Jon, S.; Kantoff, P. W.; Richie, J. P.; Langer, R. Targeted Nanoparticle-Aptamer Bioconjugates for Cancer Chemotherapy in Vivo. *Proc. Natl. Acad. Sci. U. S. A.* **2006**, *103* (16), 6315−6320.

(28) Fang, R. H.; Hu, C.-M. J.; Luk, B. T.; Gao, W.; Copp, J. A.; Tai, Y.; O'Connor, D. E.; Zhang, L. Cancer Cell Membrane-Coated Nanoparticles for Anticancer Vaccination and Drug Delivery. *Nano Lett.* **2014**, *14* (4), 2181−2188.

(29) Woythe, L.; Madhikar, P.; Feiner-Gracia, N.; Storm, C.; Albertazzi, L. A Single-Molecule View at Nanoparticle Targeting Selectivity: Correlating Ligand Functionality and Cell Receptor Density. *ACS Nano* **2022**, *16* (3), 3785−3796.

(30) Moazzam, M.; Zhang, M.; Hussain, A.; Yu, X.; Huang, J.; Huang, Y. The Landscape of Nanoparticle-Based siRNA Delivery and Therapeutic Development. *Mol. Ther.* **2024**, *32* (2), 284−312.

(31) Callmann, C. E.; Vasher, M. K.; Das, A.; Kusmierz, C. D.; Mirkin, C. A. In Vivo Behavior of Ultrasmall Spherical Nucleic Acids. *Small* **2023**, *19* (24), 2300097.

(32) Valcourt, D. M.; Day, E. S. Dual Regulation of miR-34a and Notch Signaling in Triple-Negative Breast Cancer by Antibody/miRNA Nanocarriers. *Mol. Ther.-Nucleic Acids* **2020**, *21*, 290−298.

(33) Lee, J. C.; Donahue, N. D.; Mao, A. S.; Karim, A.; Komarneni, M.; Thomas, E. E.; Francek, E. R.; Yang, W.; Wilhelm, S. Exploring Maleimide-Based Nanoparticle Surface Engineering to Control Cellular Interactions. *ACS Appl. Nano Mater.* **2020**, *3* (3), 2421−2429.

(34) Kim, Y.; Ho, S. O.; Gassman, N. R.; Korlann, Y.; Landorf, E. V.; Collart, F. R.; Weiss, S. Efficient Site-Specific Labeling of Proteins via Cysteines. *Bioconjugate Chem.* **2008**, *19* (3), 786−791.

(35) Nair, D. P.; Podgórski, M.; Chatani, S.; Gong, T.; Xi, W.; Fenoli, C. R.; Bowman, C. N. The Thiol-Michael Addition Click Reaction: A Powerful and Widely Used Tool in Materials Chemistry. *Chem. Mater.* **2014**, *26* (1), 724−744.

(36) Cengiz, B.; Ejderyan, N.; Sanyal, A. Functional Polymeric Coatings: Thiol-Maleimide 'Click' Chemistry as a Powerful Surface Functionalization Tool. *J. Macromol. Sci., Part A* **2022**, *59* (7), 443−455.

(37) Lee, N. K.; Wang, C.-P. J.; Lim, J.; Park, W.; Kwon, H.-K.; Kim, S.-N.; Kim, T.-H.; Park, C. G. Impact of the Conjugation of Antibodies to the Surfaces of Polymer Nanoparticles on the Immune Cell Targeting Abilities. *Nano Converg.* **2021**, *8* (1), 24.

(38) Marques, A. C.; Costa, P. J.; Velho, S.; Amaral, M. H. Functionalizing Nanoparticles with Cancer-Targeting Antibodies: A Comparison of Strategies. *J. Controlled Release* **2020**, *320*, 180−200.

(39) Christie, R. J.; Fleming, R.; Bezabeh, B.; Woods, R.; Mao, S.; Harper, J.; Joseph, A.; Wang, Q.; Xu, Z.-Q.; Wu, H.; Gao, C.; Dimasi, N. Stabilization of Cysteine-Linked Antibody Drug Conjugates with N-Aryl Maleimides. *J. Controlled Release* **2015**, *220*, 660−670.

(40) Smith, M. E. B.; Caspersen, M. B.; Robinson, E.; Morais, M.; Maruani, A.; Nunes, J. P. M.; Nicholls, K.; Saxton, M. J.; Caddick, S.; Baker, J. R.; Chudasama, V. A Platform for Efficient, Thiol-Stable Conjugation to Albumin's Native Single Accessible Cysteine. *Org. Biomol. Chem.* **2015**, *13* (29), 7946−7949.

(41) Shen, B.-Q.; Xu, K.; Liu, L.; Raab, H.; Bhakta, S.; Kenrick, M.; Parsons-Reponte, K. L.; Tien, J.; Yu, S.-F.; Mai, E.; Li, D.; Tibbitts, J.; Baudys, J.; Saad, O. M.; Scales, S. J.; McDonald, P. J.; Hass, P. E.; Eigenbrot, C.; Nguyen, T.; Solis, W. A.; Fuji, R. N.; Flagella, K. M.; Patel, D.; Spencer, S. D.; Khawli, L. A.; Ebens, A.; Wong, W. L.; Vandlen, R.; Kaur, S.; Sliwkowski, M. X.; Scheller, R. H.; Polakis, P.; Junutula, J. R. Conjugation Site Modulates the in Vivo Stability and Therapeutic Activity of Antibody-Drug Conjugates. *Nat. Biotechnol.* **2012**, *30* (2), 184−189.

(42) Szijj, P. A.; Bahou, C.; Chudasama, V. Minireview: Addressing the Retro-Michael Instability of Maleimide Bioconjugates. *Drug Discovery Today: technol.* **2018**, *30*, 27−34.

(43) Park, J.; Evangelopoulos, M.; Vasher, M. K.; Kudruk, S.; Ramani, N.; Mayer, V.; Solivan, A. C.; Lee, A.; Mirkin, C. A. Enhancing Endosomal Escape and Gene Regulation Activity for Spherical Nucleic Acids. *Small* **2024**, *20* (11), 2306902.

(44) Li, J.; Chen, Y.-C.; Tseng, Y.-C.; Mozumdar, S.; Huang, L. Biodegradable Calcium Phosphate Nanoparticle with Lipid Coating for Systemic siRNA Delivery. *J. Controlled Release* **2010**, *142* (3), 416−421.

(45) Yang, S.; May, S. Release of Cationic Polymer-DNA Complexes from the Endosome: A Theoretical Investigation of the Proton Sponge Hypothesis. *J. Chem. Phys.* **2008**, *129* (18), 185105.

(46) Yang, M. M.; Yarragudi, S. B.; Jamieson, S. M. F.; Tang, M.; Wilson, W. R.; Wu, Z. Calcium Enabled Remote Loading of a Weak Acid Into pH-Sensitive Liposomes and Augmented Cytosolic Delivery to Cancer Cells via the Proton Sponge Effect. *Pharm. Res.* **2022**, *39* (6), 1181−1195.

(47) Clevers, H. Wnt/β-Catenin Signaling in Development and Disease. *Cell* **2006**, *127* (3), 469−480.

(48) Xu, X.; Zhang, M.; Xu, F.; Jiang, S. Wnt Signaling in Breast Cancer: Biological Mechanisms, Challenges and Opportunities. *Mol. Cancer* **2020**, *19* (1), 165.

(49) Yang, L.; Wu, X.; Wang, Y.; Zhang, K.; Wu, J.; Yuan, Y.-C.; Deng, X.; Chen, L.; Kim, C. C. H.; Lau, S.; Somlo, G.; Yen, Y. FZD7 Has a Critical Role in Cell Proliferation in Triple Negative Breast Cancer. *Oncogene* **2011**, *30* (43), 4437−4446.

(50) King, T. D.; Zhang, W.; Suto, M. J.; Li, Y. Frizzled7 as an Emerging Target for Cancer Therapy. *Cell. Signalling* **2012**, *24* (4), 846−851.

(51) Dang, M. N.; Suri, S.; Li, K.; Gomez Casas, C.; Stigliano, G.; Riley, R. S.; Scully, M. A.; Hoover, E. C.; Aboeleneen, S. B.; Kramarenko, G. C.; Day, E. S. Antibody and siRNA Nanocarriers to Suppress Wnt Signaling, Tumor Growth, and Lung Metastasis in Triple-Negative Breast Cancer. *Adv. Ther.* **2024**, *7* (6), 2300426.

(52) Riley, R. S.; Day, E. S. Frizzled7 Antibody-Functionalized Nanoshells Enable Multivalent Binding for Wnt Signaling Inhibition in Triple Negative Breast Cancer Cells. *Small* **2017**, *13* (26), 1700544.

(53) Jho, E.; Zhang, T.; Domon, C.; Joo, C.-K.; Freund, J.-N.; Costantini, F. Wnt/β-Catenin/Tcf Signaling Induces the Transcription of Axin2, a Negative Regulator of the Signaling Pathway. *Mol. Cell. Biol.* **2002**, *22* (4), 1172−1183.

(54) Pohl, S.-G.; Brook, N.; Agostino, M.; Arfuso, F.; Kumar, A. P.; Dharmarajan, A. Wnt Signaling in Triple-Negative Breast Cancer. *Oncogenesis* **2017**, *6* (4), No. e310−e310.

(55) Cui, C.; Zhou, X.; Zhang, W.; Qu, Y.; Ke, X. Is β-Catenin a Druggable Target for Cancer Therapy? *Trends Biochem. Sci.* **2018**, *43* (8), 623−634.

(56) Ganesh, S.; Koser, M. L.; Cyr, W. A.; Chopda, G. R.; Tao, J.; Shui, X.; Ying, B.; Chen, D.; Pandya, P.; Chipumuro, E.; Siddiquee, Z.; Craig, K.; Lai, C.; Dudek, H.; Monga, S. P.; Wang, W.; Brown, B. D.; Abrams, M. T. Direct Pharmacological Inhibition of β-Catenin by RNA Interference in Tumors of Diverse Origin. *Mol. Cancer Ther.* **2016**, *15* (9), 2143−2154.

(57) Merikhian, P.; Eisavand, M. R.; Farahmand, L. Triple-Negative Breast Cancer: Understanding Wnt Signaling in Drug Resistance. *Cancer Cell Int.* **2021**, *21* (1), 419.

(58) Wang, J.; Dang, M. N.; Day, E. S. Inhibition of Wnt Signaling by Frizzled7 Antibody-Coated Nanoshells Sensitizes Triple-Negative Breast Cancer Cells to the Autophagy Regulator Chloroquine. *Nano Res.* **2020**, *13* (6), 1693−1703.

(59) Nanda, P.; JagadeeshBabu, P. E.; Gupta, P.; Prasad, A. G. Development of a Spectrophotometric Biphasic Assay for the Estimation of mPEG-Maleimide in Thiol PEGylation Reaction Mixtures. *Chem. Eng. Commun.* **2016**, *203* (11), 1464−1472.

(60) Schmid, D.; Park, C. G.; Hartl, C. A.; Subedi, N.; Cartwright, A. N.; Puerto, R. B.; Zheng, Y.; Maiarana, J.; Freeman, G. J.; Wucherpfennig, K. W.; Irvine, D. J.; Goldberg, M. S. T Cell-Targeting Nanoparticles Focus Delivery of Immunotherapy to Improve Antitumor Immunity. *Nat. Commun.* **2017**, *8*, 1747.

(61) Martínez-Jothar, L.; Doulkeridou, S.; Schiffelers, R. M.; Sastre Torano, J.; Oliveira, S.; van Nostrum, C. F.; Hennink, W. E. Insights into Maleimide-Thiol Conjugation Chemistry: Conditions for Efficient Surface Functionalization of Nanoparticles for Receptor Targeting. *J. Controlled Release* **2018**, *282*, 101−109.

(62) Chao, Y.-W.; Lee, Y.-L.; Tseng, C.-S.; Wang, L. U.-H.; Hsia, K.-C.; Chen, H.; Fustin, J.-M.; Azeem, S.; Chang, T.-T.; Chen, C.-Y.; Kung, F.-C.; Hsueh, Y.-P.; Huang, Y.-S.; Chao, H.-W. Improved CaP Nanoparticles for Nucleic Acid and Protein Delivery to Neural Primary Cultures and Stem Cells. *ACS Nano* **2024**, *18* (6), 4822−4839.

(63) Hoover, E. C.; Ruggiero, O. M.; Swingler, R. N.; Day, E. S. FZD7-Targeted Nanoparticles to Enhance Doxorubicin Treatment of Triple-Negative Breast Cancer. *ACS Omega* **2024**, *9* (12), 14323−14335.

(64) Riley, R. S.; Melamed, J. R.; Day, E. S.Enzyme-Linked Immunosorbent Assay to Quantify Targeting Molecules on Nanoparticles. In *Targeted Drug Delivery: Methods and Protocols*Sirianni, R. W.; Behkam, B.Eds., Springer, New York, NY, 2018, pp. 145−157. DOI: .

(65) Meyer-Tamaki, K. B. Chapter 21 - Preclinical Development of Monoclonal Antibodies. In *A Comprehensive Guide to Toxicology in Preclinical Drug Development*, Faqi, A. S., Academic Press, 2013, pp. 489−516. DOI: .

(66) Poole, L. B. The Basics of Thiols and Cysteines in Redox Biology and Chemistry. *Free Radical Biol. Med.* **2015**, *80*, 148−157.

(67) Wang, X.; Chu, X. Role of Surfactant in the Formation of Zein/Tween-20 Nanoparticles Studied by Fluorescence and Circular Dichroism. *Colloids Surf., A* **2018**, *558*, 110−116.

(68) Varga, N.; Bélteki, R.; Juhász, Á.; Csapó, E. Core-Shell Structured PLGA Particles Having Highly Controllable Ketoprofen Drug Release. *Pharmaceutics* **2023**, *15* (5), 1355.

(69) Tabarhoseini, S. M.; Bentor, J.; Johnson, W.; Tzeng, T.-R.; Xuan, X. Effects of Tween 20 Addition on Electrokinetic Transport in a Polydimethylsiloxane Microchannel. *Electrophoresis* **2024**, 1−5.